



**ORIGINAL ARTICLE**

## Performance of geopolymer paste as adhesive and resin material for bonding fiber externally and hardening reinforcing rebars

Marawan Ashraf Saad<sup>a,\*</sup>, Bassam Abdelsalam Abdelsalam<sup>a</sup>, Omar Mohamed Omar Ibrahim<sup>a</sup>, Hassan A. Mohamadien<sup>b</sup>

<sup>a</sup> Department of Civil and Architectural Constructions, Faculty of Technology and Education, Suez University, P.O.Box: 43221, Suez, Egypt

<sup>b</sup> Department of Civil Engineering, Faculty of engineering, Suez Canal University, Egypt

\* Corresponding Author: Marawan Ashraf Saad. Email: marawan.Saad@ind.suezuni.edu.eg

**Abstract:** Nowadays the construction of buildings confronts numerous challenges, environmentally, economically, and structurally efficiently. In addition, the saving of raw sources becomes essentially required especially for the building and construction sector. One of these solutions is based on utilizing sustainable material for construction technology. The goal of this research is to develop a more environmentally friendly material with the same performance qualities as adhesive epoxy and steel reinforcing bars. The goals of this research may be accomplished in two stages. The first step in reinforcing reinforced concrete (RC) beams is making geopolymer paste (GPP), a new kind of externally adhesive substance that may replace epoxy polymer (EP) with textiles made of synthetic glass fibers and natural jute fibers. The second advantage of GPP over PET resin for making rebars is using synthetic and natural threads, such as jute and glass fibers. In this investigation, nine reinforced concrete beams were prepared. Four of these beams were reinforced at the flexural zone with a combination of glass fiber textile (GFT) and jute fiber textile (JFT) externally bonded with epoxy or geopolymer paste. The other four specimens were reinforced with 50% GFR or JFR and 50% steel bars. In addition, one control beam is reinforced with 100% steel bars. A three-point load test is experimented on, and all RC beams are monitored up to failure. The study and analysis focused on load deflection, toughness, ductility index, and failure mechanism of beams. The theoretical ultimate load was calculated to predict and compare it to the experimental ultimate capacity of beam. According to the findings of the tests, sustainable GPP was able to harden the fiber rebars manufacturing process and serve as an externally excellent adhesive substance, on par with or even better than EP resin. The beam strengthened with jute fiber sheet that installed using GPP exhibited more cracking compared to the installation using EP resin.

**Keywords:** Geopolymer paste, epoxy resin, polyester resin, structural behavior, fiber rebars, textile fibers, strengthening technique

### 1 Introduction

A common building material, steel-reinforced concrete (SRC) boosts the material's compressive and tensile strengths by including steel rebar into the concrete mix. The main causes of age-related degradation in reinforced concrete (RC) buildings include corrosion, sulphate and acid attacks, and



freeze-thaw cycles [1, 2]. With corrosion being the most common problem, these processes drastically reduce the structures' service life. The main culprits behind the corrosion of the reinforcing components in RC are carbon dioxide and chlorides [3, 4]. To combat this corrosion problem, specialists have begun using fiber-reinforced polymer (FRP) bars, which are composites made of fibers embedded in polymeric resin [5-8]. Since FRP is neither a metal nor an electromagnetic interference, using it as reinforcement removes any concerns about metal corrosion. Also, FRP materials are great for structural reinforcement because of their high levels of residency. These consist of low electrical conductivity, strong tensile strength, corrosion resistance, low weight, and the ability to avoid producing electromagnetic fields [9-14]. One common method in rehabilitation is to utilize an externally bonded (EB) fiber-reinforced polymer (FRP) system that is based on epoxy resin. In this technique, the fibers are oriented perpendicular to the longitudinal axis of the RC portion. Corrosion resistance, high strength, and little maintenance needs are just a few of the reasons why FRP is quickly becoming the go-to method for rehabilitation projects [15-21]. Epoxy resin has considerable drawbacks that prevent it from being developed further as a system for reinforcing concrete structures. These include low performance at high temperatures, incompatibility with masonry and concrete, and the fact that it causes FRP laminates and RC concrete surfaces to debond due to the adhesive material's weak cohesion [22-25]. To solve the issues related to resin consumption while keeping the advantages of fiber-reinforced plastic (FRP) applications, composite systems that use inorganic, eco-friendly mortar as binders instead of resin have been developed [26-29]. A number of new technologies, such as textile-reinforced concrete (TRC), mineral-based composite (MBC), and textile-reinforced mortar (TRM), have recently been introduced to the construction sector as alternatives to FRP [30-36]. In FRCM composites, the matrix and binder are fabric grids made of fibers such as carbon, glass, etc., and cementitious agents, also known as mortar. The matrix used in fabric-reinforced cementitious matrix (FRCM) composites is better at withstanding heat and is more compatible with concrete than epoxy resin, which is used in FRP. To make the system more compatible with the concrete base and increase its heat and fire resistance, mortar might be used instead of epoxy [37, 38]. Polymer-treated concrete mortars are the recommended material for TRM strengthening. While polymer-modified cement mortar enhances cohesiveness between the concrete foundation and reinforcing layers, additional study reveals that the connection degrades dramatically when exposed to fire. This is in contrast to the reinforcing effects of regular cement mortar. Hu [39, 40] investigated the fire resistance of TRM-strengthened slabs using polymer-modified cement mortar as the binder. After 30 minutes in the fire, the strengthening layer peeled off, which isn't long enough for most uses, according to his findings. Repair mortars made of cement have low fire resistance and low binding strength, thus finding a suitable substitute is crucial. Geopolymer has garnered a lot of attention in the last few decades due to its potential to replace cement. It is an environmentally benign substance that has the same or even better properties than cement [41-43]. The method that results in geopolymer is the mixing of alkaline solutions, such NaOH or KOH [44-46]. Materials with a lower calcination temperature are often employed as aluminosilicate source materials. Rice husk ash, metakaolin (MK), and fly ash are all part of this category of materials. It is possible for employees to provide services using the material to suffer burns and other issues due to its high alkalinity [47-49]. To finish the chemical processes that enhance the mechanical qualities of conventional and geopolymer concrete, fly ash (FA), a fine mineral substance composed of silica and alumina oxides, requires thermal curing [50]. The manufacture of geopolymers produces less carbon dioxide and uses less energy as a consequence. Geopolymer is being considered as a possible substitute for cement due to its exceptional qualities, such as its quickness to set, strong early compressive strength, and exceptional fire resistance [45, 46, 51-53]. As an alternative to cement paste, geopolymer paste works just as well. The binding strength, early high strength, heat resistance, and other cement binder properties are also shown by geopolymer binders [54, 55]. Cement concrete attributed to FA or MK forms a high network into the alkali-activated matrix, although geopolymer concrete based on these materials exhibited reduced drying shrinkage, greater indirect tensile strength, and higher modulus of elasticity [56].

Corrosion may occur on steel reinforcement at any time because of various environmental variables. With this goal in mind, come up with creative solutions to the problem of finding appropriate materials to substitute steel reinforcing bars. However, one option is to boost the concrete capacity by reinforcing concrete parts using sustainable materials. The reinforcement was made of fiber-reinforced polymer (FRP) bars. It is required to find more sustainable, eco-friendly, and cost-effective alternatives

to epoxy polymer (EP) resin because of all the problems it causes in rebar production and external bonding. This research compares an epoxy-based method with geopolymer paste (GPP) to connect fiber textiles to concrete surfaces (externally bonding reinforced concrete). Rebars made of both natural and synthetic fibers may be hardened in part by using GPP as a resin ingredient. The present study aims to investigate the effectiveness of using a GPP for bonding purposes between fiber textile and concrete surface (strengthening reinforced concrete with the externally bonded system), compared to the epoxy-based system. One aspect involves utilizing GPP as resin material to harden the natural and synthetic fiber rebars.

## 2 Experimental program

### 2.1 Preparation and specimen details

The experimental work includes nine reinforced concrete beams divided into two phases. Concrete materials, adhesive and hardened materials, and reinforcement details are presented and discussed. **Fig. 1** shows the experimental schematic of reinforced concrete beams.

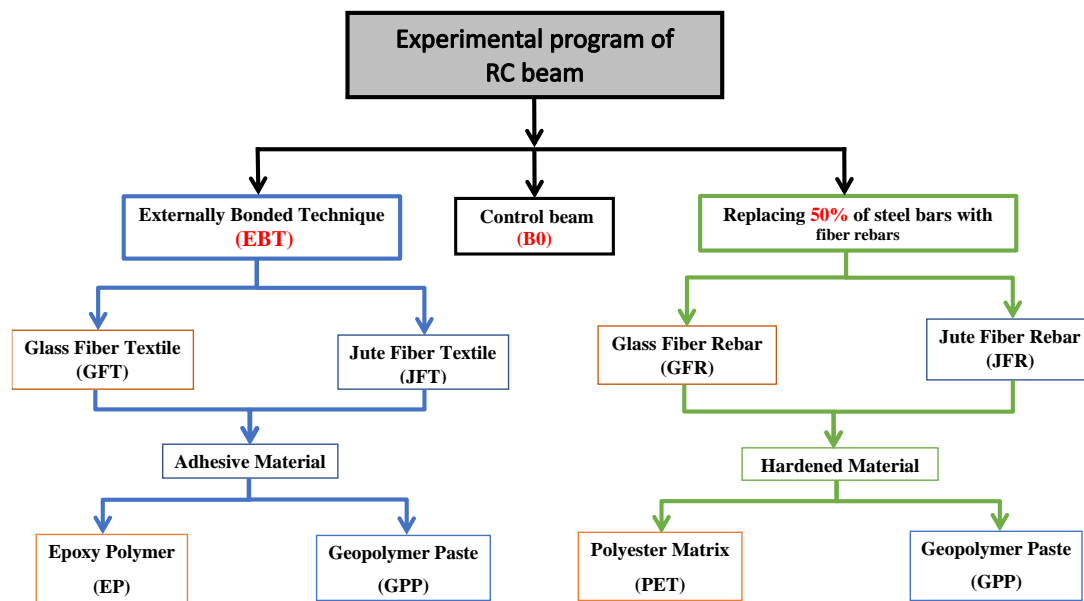


**Fig. 1.** Experimental schematic of RC beams

#### 2.1.1 Concrete materials

Ordinary Portland cement OPC CEM I 42.5N was used conforms to the requirements of the specification mentioned [57]. The cement properties are presented in **Table 1**. Natural fine and coarse aggregates (sand and crushed stone) were utilized for concrete mix. The specific gravity of sand and crushed stone was 2.63 and 2.67, respectively. The particles size distribution of aggregates is carried out in accordance with [58]. A high-performance superplasticizer (Viscocrete-3425) concrete admixture was used to improve the flowability of concrete mixtures and reduce the water content. The superplasticizer has a specific gravity of 1.08 and complies with [59]. A uniform concrete mix with a compressive strength of 42 MPa was designed for all RC beams. The concrete mix includes a 350 kg/m<sup>3</sup> cement, 1:1.5 fine to coarse aggregate, 0.3 water to cement ratio, and 2% superplasticizer. The mixes were designed and implemented in accordance with ACI 211.4R-08 [60].

#### 2.1.2 Adhesive and hardening materials

##### 2.1.2.1 Epoxy polymer (EP) resin

The two-part product, Kemapoxy 165 adhesive mortar, is based on modified epoxy resin and has a suitable hardening mechanism. It was sourced from Chemicals Modern Building (CMB). This product conforms with ASTM C 881 [61] and has technical details that are detailed in **Table 2** of the

manufacturer's specifications. As an external bonding strengthening technique, RC beams had layers of GFT and JFT installed using epoxy resin in the flexural zone at the bottom. On the other hand, the matrix material for hardening both the GFR and the JFR is typically polyester (PET) resins. In order to make the composite strong and long-lasting, the matrix material bonds and shields the reinforcing fibers. One portion of the two-component, transparent, and liquid impregnating resin was polyester ES 1319, which has a medium viscosity.

**Table 1.** Properties of cement and Fly ash materials

Properties	Cement	Fly ash
<b>Physical properties</b>		
Specific gravity	3.15	2.50
Specific surface area (cm <sup>2</sup> /gm)	3250	3950
Color	Gray	Light gray
<b>Chemical compositions (%)</b>		
SiO <sub>2</sub>	20.30	61.06
Al <sub>2</sub> O <sub>3</sub>	6.46	28.55
Fe <sub>2</sub> O <sub>3</sub>	3.66	3.15
CaO	62.15	1.41
MgO	3.32	1.32
SO <sub>3</sub>	2.51	1.06
K <sub>2</sub> O	0.75	-
Na <sub>2</sub> O	0.85	-

**Table 2.** Properties of EP resin and GPP matrix

Properties	Epoxy	Geopolymer
Color	Grey	Dark grey
Solid content	100%	100%
Density (g/cm <sup>3</sup> )	1.95 ± 0.02	1.84
Mixing ratio, A:B (by weight)	12: 1	-
Compressive strength (ASTM D 695) (N/mm <sup>2</sup> )	80	35.6
Tensile strength (ASTM D 695) (N/mm <sup>2</sup> )	-	8.16
Flexural strength (ASTM D 790) (N/mm <sup>2</sup> )	> 40	-
Punching sheet strength (ASTH D732) (N/mm <sup>2</sup> )	25	-
Adhesive strength on concrete (ASTM C 882) (N/mm <sup>2</sup> )	10.3	1.96

#### 2.1.2.2 Geopolymer paste (GPP)

There are two main components for preparing GPP: fly ash and alkaline solution. Low-calcium fly ash (FA) class F satisfying the requirements of ASTM C618 [62] was used as a source material for geopolymer studies. The chemical compositions and physical properties of the FA are presented in **Table 1**. The material had an average particle size of 28 microns.

An alkaline solution (AS) was prepared as an activator material to produce the GPP that consisted of two component materials, sodium hydroxide solution (SHS) and sodium silicate solution (SSS). Sodium hydroxide pellets form with 99% purity and a molecular weight of 40, were acquired from (El Nasr for Intermediate Chemicals). These pellets were used to prepare the AS that is used in geopolymer as the activator. The SSS was obtained from the Egypt Global Silicates company and had the following chemical ratios: 60% water content, 9% Na<sub>2</sub>O, and 31% SiO<sub>3</sub>, Molecular Weight 184 – 254, Weight Ratio 1:2.

A SHS with a molarity concentration of 12 M was prepared by dissolving sodium hydroxide granules in tap water 24 hours before use to lower the ambient temperature. It was then mixed, in a mass proportion of 2.5 with a SSS to create an alkaline activator solution, accelerating the reaction of the solution. The liquid-to-binder ratio was chosen as 0.7 to achieve high fluidity, aiding the penetration of the dough between the fiber strands and accelerating absorption.

The mixing process of GPP is conducted as follows: the fly ash was initially placed into the mixing machine, followed by the gradual pouring of the pre-prepared alkali activator. The mixing continued

for about 3 minutes until the dough appeared homogeneous and attained the desired consistency. All samples were cured at an ambient temperature of 23 °C and 50% relative humidity until the testing time. The 28-day average compressive strength was determined using six 50×50×50 mm cube samples. **Table 2** shows the properties of adhesive materials corresponding to ASTM D7205-06 [63]. The GPP was prepared to bond the external fiber sheets for strengthening RC beams and hardening the fiber rebars for a main bottom reinforcement of RC beams.

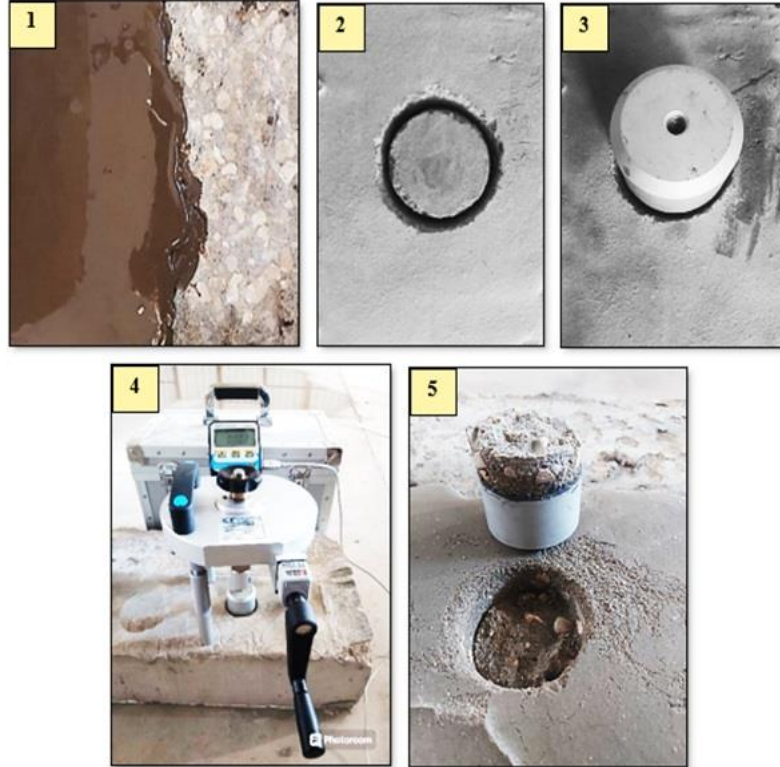


**Fig. 2.** Experimental sequences of pull-off test of GPP overlay

According to the BS EN 1542:1999 standard [64], tensile testing techniques are employed to ascertain the repair overlay's adherence to the concrete substrate, as presented in **Fig. 2**. The pull-off test pertains to one such method. The foundation of the structure was made of 100 mm thick, 1000 mm × 250 mm unreinforced concrete slabs. Wet burlap sacks were placed over the slabs and specimens for a period of two days. Following this curing phase, the slab specimen was demoulded and stored in a standard laboratory setting. After 28 days of aging on the concrete substrate, the casting surface—the top surface of the slab specimen—had to be treated. Roughing the top surface of a concrete substrate involves removing a very small layer of the surface in order to produce an uneven surface. This process also eliminates trash, oils, and grease. Once the bond compound was in place, the new concrete overlay could be cast. The freshly mixed geopolymer mortar overlay was firmly fastened to the hardened concrete in accordance with the procedures specified in Egyptian Code No. 203[65]. Pull-off tests were carried out after the geopolymer mortar overlay had cured for about 28 days. Reason being that evaluations of pull-off strength are the purview of instrumental characteristics. The following formula is used to find the tensile bond strength (to the nearest 0.1 MPa) for every test location that produces a typical failure. To arrive at the BS EN 1542:1999 standard, a series of computations were performed [64]:

$$fh = 4 F_h / \pi D^2 \quad (1)$$

Where ( $fh$ ) is the bond of the test specimen, in megapascals; ( $F_h$ ) is the failure load, in Newtons; and ( $D$ ) is the main diameter of the test specimen, in millimeters.

### 2.1.3 Reinforcement materials

The reinforcement details in this work are designed for two purposes. First, internal reinforcement of concrete beams using three types of reinforcement materials which were steel reinforcement bars, GFR, and JFR. Second, external reinforcement as strengthening concrete beams using two types of fiber textile laminates GFT and JFT that being bonded by EP resin or GPP with concrete substrate.



(a) GFR



(b) JFR

**Fig. 3.** Fiber rebars production process.

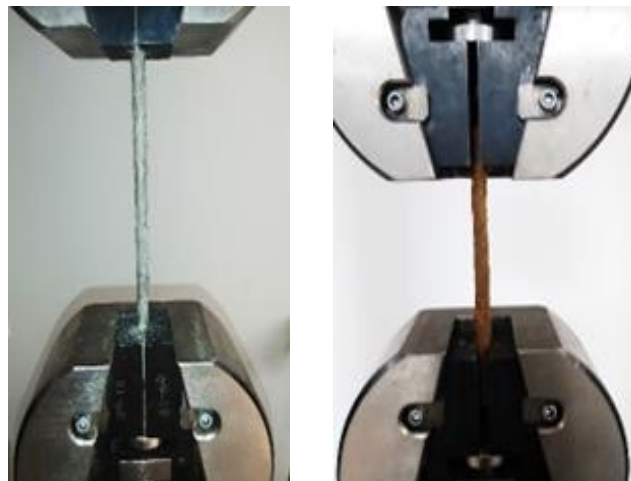


**Fig. 4.** Tensile test of fiber rebars

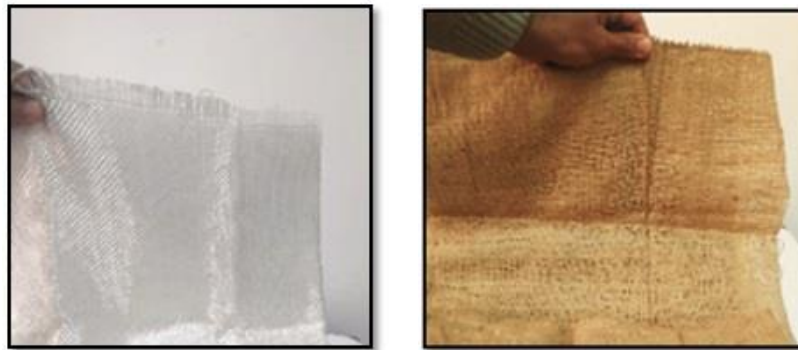
For internal reinforcement, the concrete elements were designed with 2Ø8 mm as main steel reinforcement bars at bottom of beam. The steel reinforcement was mild steel bars grade B240C-P ESS, and the engineering properties of steel bar was experimented according to the Egyptian standard specifications 262/2015. The GFR with 8 mm diameter was utilized as internal reinforcement by 50% of the main steel reinforcement of concrete beam. The GFR was produced from synthetic glass fiber threads using a rope-making machine and the hand lay-up technique up to the required diameter, then hardening the GFR using two techniques. The first technique of hardening process is PET resin with treated the rebar surface using sand aggregate to improve bond strength with concrete. The second

hardening technique is GPP which prepared as mentioned previously. The last internal reinforcement type is JFR by diameter of 8 mm that utilized as 50% replacement of steel reinforcement bars. The natural jute fiber thread is the main material to produce rebar by the same sequence process of producing GFR. The fiber rebars production process includes initially filling the machine with an appropriate quantity of fibers to achieve the desired diameter and hardening the rebars using a matrix of each PET or GPP, as presented in Fig. 3. The mechanical characteristics of the internal reinforcement (steel bars, GFR, and JFR) are conducted in accordance with the ASTM D7205-06 [66], which tabulated in **Table 3**. The tensile test of fiber rebars are experimented with, as shown in **Fig. 4**.

**Table 3.** Mechanical properties of steel, Rebar reinforcement.

Property	Steel bars	Fiber rebars			
		GFR-EP	GFR-GPP	Jute-EP	Jute-GPP
Diameter (mm)	8	8	8	8	8
Initial gauge length (mm)	80	200	200	200	200
Final gauge length (mm)	102.29	200.6	200.7	200.5	200.4
Maximum load (N)	22600	32418	25934	7178	8343
Maximum tensile stress (MPa)	449.61	645	516	143	166
Yield tensile stress (MPa)	328.57	-	-	-	-
Tensile stress / Yield Stress	1.37	-	-	-	-
Elongation (%)	21.79	11.86	9.49	5.53	6.34
E- modulus (GPa)	193	-	-	-	-

For external reinforcement, GFT and JFT layers are 100 mm width and 500 mm length. The utilized synthetic textile fiber is alkali-resistant glass fiber, and the natural textile is jute fiber mesh, as shown in **Fig. 5**. The mechanical properties of GFT based on the manufacture of glass fabric mesh are shown according to data from the manufacturer which conform to EN15422:2008 [67] for glass mesh fabric and fiber glass thread, respectively. **Table 4** lists the mechanical properties of the jute fiber used in the manufacture of jute fiber-reinforced polymer (JFRP) and jute fiber-reinforced geopolymer (JFRGP) bars and the jute Fabric of mesh, used in external bonded reinforcement (EBR).



(a) GFT

(b) JFT

**Fig. 5.** Fiber textile sheets.

**Table 4.** The Mechanical properties of Synthetic fibers and Natural fibers.

fibers	Modulus of elasticity (GPa)	Ultimate tensile strength (MPa)	Specific gravity g/m <sup>3</sup>
Glass fiber	-	1700	2.7
jute fiber	-	432	1.52
glass sheet	80.4	1290	2.7
jute sheet	17.85	328	1.52

#### 2.14 Specimens' preparation

Nine simply supported beams are designed for flexure test with three-points load type. The overall prism dimensions are 100×100×700 mm. The RC beams were designed as singly reinforced section using 2Ø8 mm mild steel bars. The main steel reinforcement was placed at an effective concrete depth

of 80 mm. The beam samples were designed according to ACI 318–14[68] and ACI 440.1R-15 [69]. The reinforcement details of the tested beams are illustrated in **Table 5**.

**Table 5.** Reinforcement details of tested beams

Beam ID	Definition	Main reinforcement			EBR	
		Steel	Rebars		Fiber Sheet	
			GFR	JFR	GFT	JFT
B0	Control	2Ø8 mm	-	-	-	-
G1	B1-GFT-EP	2Ø8 mm	-	-	100×600 mm	-
	B2-GFT-GPP		-	-	100×600 mm	-
	B3-JFT-EP		-	-	-	100×600 mm
	B4-JFT-GPP		-	-	-	100×600 mm
G2	B5-GFR-EP	1Ø8 mm	1Ø8 mm	-	-	-
	B6-GFR-GPP	1Ø8 mm	1Ø8 mm	-	-	-
	B7-JFR-EP	1Ø8 mm	-	1Ø8 mm	-	-
	B8-JFR-GPP	1Ø8 mm	-	1Ø8 mm	-	-

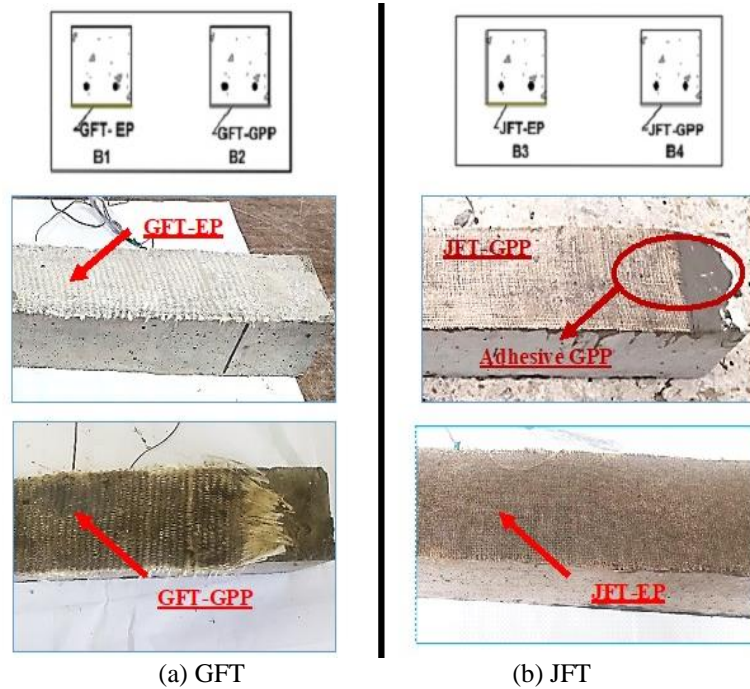


**Fig. 6.** Beams strengthened externally with fiber sheet.

All concrete elements were cast, compacted, and cured for 28 days before subjected to flexural loading process. The RC beams were categorized into two groups in addition control beam (B0), each comprising four specimens. The first group involved strengthening the RC beams using external reinforced system based on one layer of each GFT sheet or JFT sheet which bonded with two techniques either EP resin or GPP matrix. **Fig. 6** shows the strengthening and installation process of the fiber sheets externally on the RC beam. In the second group, the RC beams were reinforced internally with 50% of steel bar (1Ø8 mm) and 50% of fiber rebar (1Ø8 mm). The fiber rebars variables were GFR hardened with whether PET resin or GPP matrix, and JFR hardened with PET resin or GPP matrix. The steel

reinforcement bars were 100% in control specimen and the strengthened beams but replaced with 50% for other RC beams, as presented in Fig. 7. The main properties of rebars are lower than the properties of steel bars, therefore the concrete beams will redistribute the moment along the beam. Because of the uneven cross-section, the beam exhibits non-linear behavior, particularly when subjected to greater stress. A precise prediction of the moment distribution may therefore be beyond the scope of the linear elastic analysis.

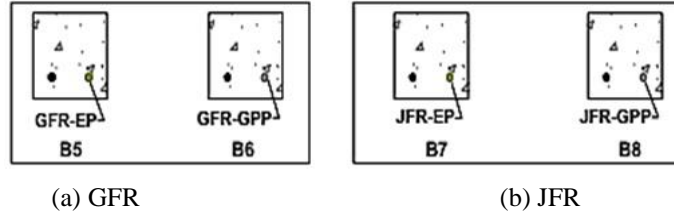


Fig. 7. Beams reinforced internally with 50% fiber rebar.

The sequence of strengthening beams externally were as follows: initially, clean the outer surface of the bottom beam, then cut both of glass fiber sheet and jute fiber sheet with dimension of 100 mm width and 600 mm length before glued at the bottom surface of RC beam, next placing and distribute the adhesive material whether EP resin or GPP matrix on the bottom surface area (100×600 mm), then installing the one layer of fiber sheet either GFT or JFT with 100% of the clear tested span (500 mm), lastly, keep the samples after strengthened for 24 hrs. at room temperature to continue the hardened process and getting a better performance. On the second phase, the reinforcing beams with 50% of steel bar and 50% of fiber rebar were carried out before casting the concrete mix into the moulds.

2.2 Test Setup

The RC beam samples were loaded using a three-point load according to ASTM C78 [70] on a universal testing machine with a maximum capacity of 1500 kN and the loading rate was 15 mm/min. The RC beams with an effective span of 500 mm were subjected to a static load. One dial gauge with 0.01 mm accuracy was installed under the bottom beam at the middle span through loading process. The schematic diagram of the test setup was presented on Fig. 8. The load and deflection were recorded gradually up to failure.

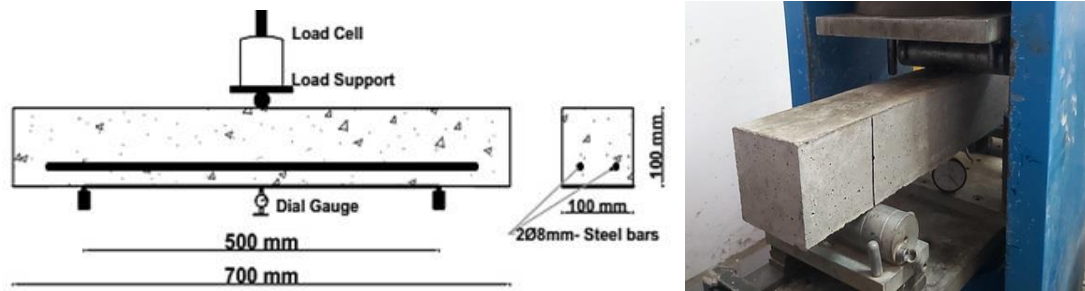


Fig. 8. Test setup, dimensions, and reinforcement details of RC beams.

Table 6. Experimental and theoretical results of RC beams.

Beam ID	Loads (kN)				$P_{u/Exp} / P_{u/Theo}$	$\Delta_{max.}$ (mm)	$\mu$	Toughness (kN.mm)	
	$P_{cr}$	$P_y$	$P_{u/Exp.}$	$P_{u/Theo.}$					
B0-Control	5	22.5	27	21.2	1.27	6.20	2.70	132.97	
G1	B1-GFT-EP	8	26	30	37.2	0.81	12.57	1.85	287.98
	B2-GFT-GPP	13	28	30	37.2	0.81	8.44	2.64	211.29
	B3-JFT-EP	8	23	32	34.1	0.94	9.26	4.63	258.03
	B4-JFT-GPP	8	27	32	34.1	0.94	7.22	3.01	198.38
G2	B5-GFR-EP	6	10	20	17.7	1.13	4.5	1.80	68.60
	B6-GFR-GPP	7	11	16	16.4	0.98	3.5	7.00	47.02
	B7-JFR-EP	4	10	14	15.5	0.90	3.0	2.73	43.33
	B8-JFR-GPP	8	14	16	16.2	0.99	4.0	5.00	62.20

Note:  $P_{cr}$ : Crack load;  $P_y$ : Yield load;  $P_{u/Exp.}$ : Experimental ultimate load;  $P_{u/Theo.}$ : Theoretical ultimate load;  $\Delta_{max.}$ : Maximum deflection;  $\mu$ : Ductility index

### 3 Results and discussion

The experimental test and theoretical results were recorded and calculated as presented in **Table 6**. The experimental results include load-deflection behavior, toughness, ductility index, and failure modes.

#### 3.1 Load-deflection behavior

The beams were visually inspected until the first crack showed up, and the correct cracking load and final deflection were determined. Different load-deflection curves were observed in the beams analyzed using rebar, external-bonded reinforced (EBR), and reference beams in lieu of reinforcing bars. The experimental load-deflection curves for each tested beam are shown in **Figs. 9** and **10**. In most cases, these curves are characterized by three primary branches. The first, linear branch describes the reaction until the initial fractures appear. The second branch, which is likewise linear but has a smoother slope, shows the reaction up to the longitudinal reinforcement yield. As the third branch, fracture settlement, progressed to failure, the load decreased noticeably at each newly developed gap [71]. **Fig. 9** displays the load-deflection curves for beam specimens secured with EP resin adhesives and the control beam (B0). Summarized in **Fig. 10** are the yield and ultimate loads for each beam. Two bonding procedures seemed to work equally well—epoxy resin and geopolymer basting—because the beams broke at the same final stress circumstances. The load-carrying capacity of beams strengthened externally is often greater than that of non-strengthened ones [72]. While the control beam failed at 27 kN ultimate stress, beams reinforced with glass fiber sheets, geopolymer paste, and epoxy resin failed at 30 kN. Reinforced beams using geopolymer basting, epoxy adhesive, and jute fiber sheets broke at a 32 kN ultimate load. With jute fiber sheets, the ultimate load is 18.51% more than with glass fiber sheets, and with the control beam, it is 11.11% higher. For variable groups B1-B4 reinforced by the external bonding method, the ultimate loads of different adhesives with the same fabric are almost the same but the yield loads differ. The yield/ultimate loads ratios were 86.7, 93.3, 71.9, and 84.4% for specimens B1, B2, B3, and B4, in sequence. This result revealed that using jute textiles with epoxy gains the beam good beam behavior and prediction prior to failure due to the better bond efficiency between the jute textile and each EP and GPP. The bigger the ratio after the steel yields, the greater the load that the beam can sustain before failure and avoid sudden failure [73]. The strengthened beams exhibited greater deflection at ultimate load compared to the control beams, as shown in **Fig. 9a**. The deflection at ultimate load in the beams reinforced with GFT was 8.44 mm and 12.57 mm for beams using GPP matrix and EP resin, respectively compared to a deflection of 6.2 mm in the control beam. This represents an increase in deflection by 36.13% to 102.74%. For beams reinforced with JFT, the maximum deflection was 9.22 and 7.22 mm for specimens B3-JFT-EP and B4-JFT-GPP, respectively, as shown in **Fig. 9a**. This is higher than that of the control beam by an increase of 48.7% and 16.45%. In addition, the structural behavior of the beams strengthened using GFT and JFT that installed with GPP matrix were very close to each other, which means that GPP matrix is suitable for this strengthening system with different fiber types.

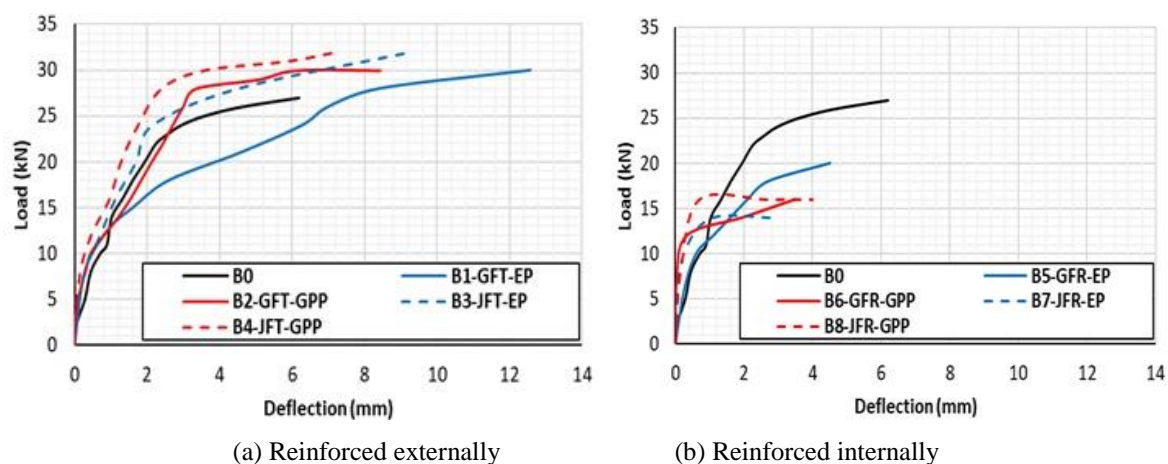


**Fig. 9.** Load-deflection behavior of the EBR technique.

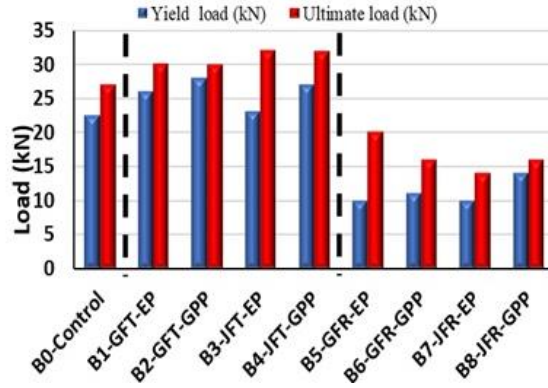


Fig. 10. Yield and ultimate loads of the tested beams

Ultimate loads of 20 kN and 16 kN for beams B5-GFR-EP and B6-GFR-GPP were reached before beams reinforced with GFR hardened with GPP matrix failed. In comparison to the control beam, this represented a reduction of 24.92% and 40.74%, correspondingly. In comparison to the control beam reinforced with epoxy resins (48.14% decrease in ultimate load) and geopolymer paste (40.74% reduction in ultimate load), jute rebar-reinforced beams failed at ultimate loads of 14 kN and 16 kN, respectively, as shown in Fig. 9b. Deflections at the ultimate load were different for the control beams and specimen reinforced with 50% of GFR, as shown in Fig. 9a. With PET resins, the maximum load deflection in GFRP beams was 4.5 mm; with hardener GPP matrix, it was 3.5 mm, a decrease of 27.41-43.54%. The use of epoxy resins resulted in a 3 mm deflection under ultimate load for jute rebar beams, whereas geopolymer paste caused a 4 mm deflection Fig. 9b, which corresponds to a decrease of 51.61-35.48%. The ultimate load for beams reinforced with GPP matrix as a binder for reinforcement rebar was similar for both types of fibers used, at an ultimate load of 16 kN, as shown in Fig. 9b. Geopolymer paste rebars showed increased deflection and load compared to epoxy resin bars with jute fibers, confirming the success of geopolymer paste as an adhesive and reinforcing material for both natural and synthetic fiber-reinforced bars.

### 3.2 Theoretical analysis

The theoretical analysis were carried out according to procedures specified in Egyptian Code Practice ECP203 [65], and the correlation factors of the ultimate load between experimental and theoretical results for strengthening and control beams are listed in Table 6. The stress-strain diagrams of the experimental specimens were clarified on Fig. 11. The theoretical results were obtained based on the following formulas:

$$C = T \quad (2)$$

$$2f_{cu} \cdot a \cdot b / 3 = A_s \cdot f_y \quad (3)$$

$$M_u = (A_s \cdot f_y) \times (d - a / 2) \quad (4)$$

$$A_{s_{min.}} = 1.1 \cdot b \cdot (d f_y) \quad (5)$$

$$(A_s \cdot E_s \cdot \varepsilon_s) + \left( A_f \cdot E_f \cdot \frac{\varepsilon_{fe}}{\gamma_f} \right) = \frac{2}{3} f_{cu} \cdot a \cdot b \quad (6)$$

$$M_u = \left[ (A_s \cdot E_s \cdot \varepsilon_s) \times (d_1 - c) \right] + \left[ \left( A_f \cdot E_f \cdot \frac{\varepsilon_{fe}}{\gamma_f} \right) \times (d_2 - c) \right] + \left[ \left( \frac{2}{3} f_{cu} \cdot a \cdot b \right) \times \left( c - \frac{a}{2} \right) \right] \quad (7)$$

Where ( $C$ ) is the compression force, ( $T$ ) is the tension force, ( $f_{cu}$ ) is the concrete compressive strength, ( $a \cdot b$ ) is the equivalent cross-section area that subjected to compression stress, ( $A_s$ ) is the area of steel bars, ( $f_y$ ) is the yield tensile stress if steel bars, ( $M_u$ ) is the bending moment of the concrete beam, ( $d$ ) is the effective depth of concrete beam. ( $A_{s_{min.}}$ ) is the minimum area of steel of the beam. It can be seen from calculations that the section includes steel reinforcement that is not less than the minimum area of steel. The calculations display that the beam is under a reinforced section, ( $E_s$ ) is the elastic modulus of steel bars, ( $\varepsilon_s$ ) is the strain of steel bars, ( $d_1$ ) is the depth of beams at internal main

reinforcement,  $(c)$  is the value of neutral axis from top beam,  $(A_f)$  is the cross-section area of external fiber layer,  $(E_f)$  is the elastic modulus of external fiber textile,  $(\epsilon_{fe})$  is the strain of fiber textile,  $(\gamma_f)$  is the reduction factor of fiber sheet,  $(\gamma_c)$  is the reduction factor of concrete,  $(d_2)$  is the depth at external fiber sheet.

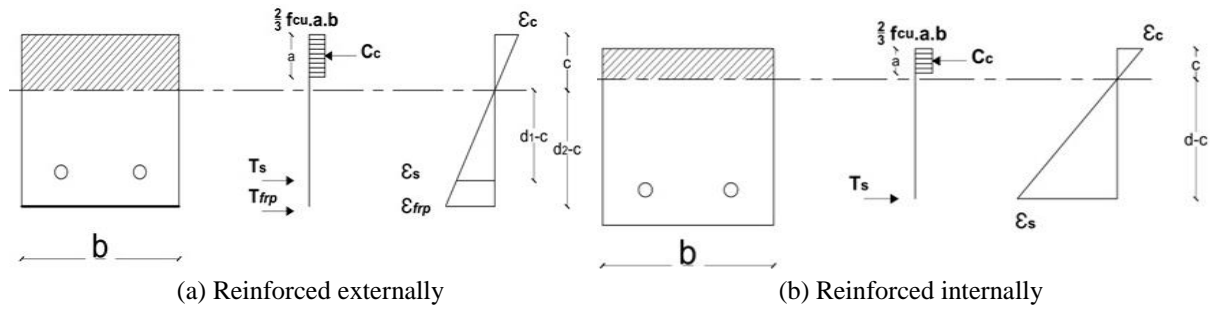


Fig. 11. Stress-strain diagram of RC beams.

The limit state of collapse is a common basis for the ultimate load prediction since it accounts for the greatest load-carrying capability and guarantees safety. Materials mechanics, structural analysis, and material characteristics provide the bulk of the theoretical basis. Reinforcement materials with stress-strain relationships include concrete, steel bars, and fiber ropes. Usually, steel exhibits elastic-perfect plastic behavior, with yield strength serving as the tipping point. In order to determine flexural capacity, one must find the moment of application that is balanced between the tensile and compressive stresses in reinforcement and concrete, respectively, as presented in Fig. 11b. Predicting the ultimate moment capacity is made easier by linking the applied bending moment to the beam's curvature.

There are extra considerations when predicting the ultimate load of reinforced concrete beams reinforced with fiber-reinforced polymer (FRP) sheets because of the interaction between the original RC beam and the externally bonded FRP material. The composite action between RC beam and FRP sheets is included to evaluate the flexural capacity of beams strengthened externally, as displayed in Fig. 11a. There is a strong correlation between the ultimate load and the FRP material's characteristics and its connection with concrete. FRP revealed little ductility and strong tensile strength; behaves linearly elastically until failure. This theoretical basis enables accurate prediction of ultimate loads, ensuring both safety and efficiency in design.

As presented in Fig. 12, the correlation factor of experimental to theoretical ultimate load ( $P_{u,Exp}/P_{u,Theo.}$ ) of most specimens was considerable nearest. The maximum difference ratio was 27.4% for control beam B0. The factors of strengthening beams group were 81% and 94% for beams strengthen with GFR and JFR, respectively. However, the beams reinforced internally with composite reinforcement achieved the correlation factors of 1.13, 0.98, 0.90, and 0.99 for specimens B1-GFR-EP, B2-GFR-GPP, B3-JFR-EP, and B4-JFR-GPP, in sequence. This comparison referred to the good prediction of ultimate load capacity theoretically and matching with experimental findings.

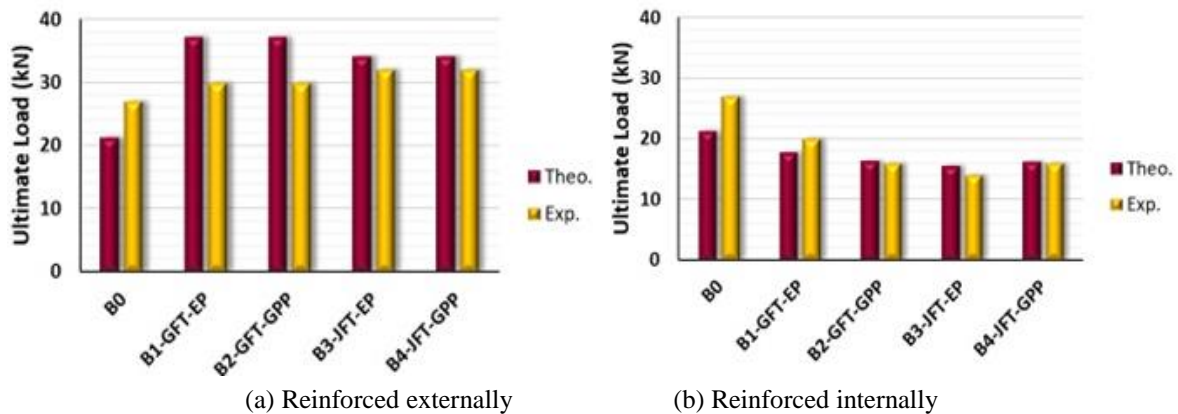
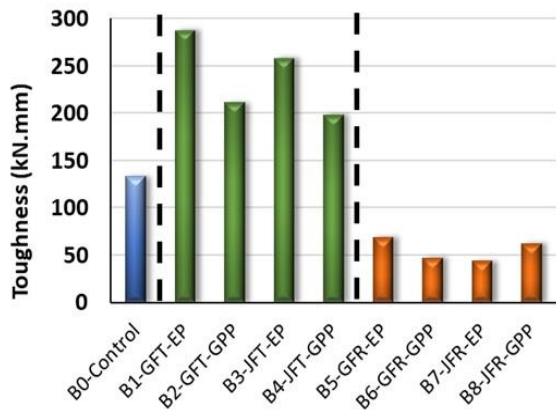


Fig. 12. Relationship of ultimate load between experimental and theoretical results.

### 3.3 Toughness

Toughness is measured by areas under the load-deflection curve, which indicates the specific test specimen's energy absorption capabilities. As a result, the size of this measure is directly related to the specimens and the loading system's geometrical properties [74]. **Table 6** represents the toughness result for the tested samples. EBR with GFT exhibited an increase in toughness of 116.6% and 58.9% for B1-GFT-EP and B2-GFT-GPP, respectively, compared to the control sample. Similarly, the incorporation of JFT led to toughness increasing by 94.0% and 49.2% with B3-JFT-EP and B4-JFT-GPP, respectively, as shown in **Fig. 13**. After comparing the control beam and the other beams reinforced using GPP, it is clear that beams strengthened with fiber sheets (both GFT and JFT) using epoxy resin enhance the toughness of RC beams. Based on these findings, epoxy seems to have superior flexural toughness compared to geopolymer. On the other hand, installing fiber laminates using GPP revealed good efficiency and higher toughness of RC beams by ratios of 58.9% and 49.2% than the control beam B0.



**Fig. 13.** Toughness of beams

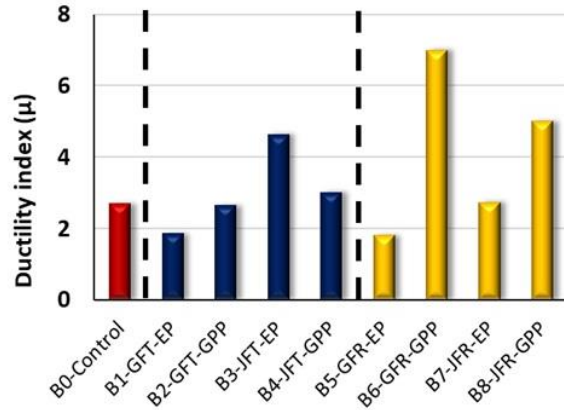


**Fig. 14.** Ductility index of beams

Beams B6-GFR-GPP and B5-GFR-EP recorded the lowest toughness by 64.6% and 48.4%, respectively, for materials reinforced with GFR. The reduction for JFR-reinforced components reached 67.4% for B7-JFR-EP and 53.2% for B8-JFR-GPP, respectively (**Fig. 13**). Rebars hardened with GPP matrix samples were just as tough as specimens hardened with PET resin. The beams reinforced with hybrid reinforcement display better performance than non-reinforced beams, but the toughness of the beam may be lower than that fully reinforced with steel reinforcement bars [75]. Fiber rebar-reinforced samples may have noticeably less toughness than the control specimen because of the rebar's high deformation and non-linear elasticity. The large replacement percentage of fiber rebars rather than the steel reinforcing bars might also be to blame.

### 3.4 Ductility index

**Table 6** provides a summary of the ductility indices ( $\mu$ ) of all the tested beams. In this study, the ductility index ( $\mu$ ) is calculated by dividing the deflection at the ultimate load by the deflection at the yield load based on the load-deflection curve of each specimen [76], as follows formula:

$$\mu = \Delta_{pu} / \Delta_{py} \tag{8}$$

Where:  $\Delta_{pu}$  is the deflection at ultimate load, and  $\Delta_{py}$  is the deflection at yield load.

As  $\mu$  values of the control beam and EBR beams are visually presented in **Fig. 14**. Specimen B3-JFT-EP showed the maximum improvement ratio of 71.8% compared to control sample B0; this improvement was achieved by reinforcing the beam externally with a JFT sheet glued with EP resin. In comparison to traditional RC beams and steel fiber RC beams, fiber-reinforced concrete beams with outside GFRP laminates show an 87% reduction in ultimate deflection, according to Mariappan Mahalingam et al. [77]. Moreover, the external strengthening using JFT glued with GPP also develops the ductility of beam by 11.5% compared to control beam. The GPP may need more treatment after casting to improve the installation efficiency through loading tests. All beams strengthened externally from B1 to B4 revealed better deformation than the reference beam, according to load-deflection behavior. Although the fiber sheets increased the ultimate capacity of RC beams, the stiffness of beams decreased, therefore the ductility index was affected positively or negatively.



internally using 50% fiber rebars and 50% steel bars clarify the superiority of GPP as hardener material for each fiber rope GFR and JFR compared to PET hardener material. The ductility of hybrid beams improved by 37% to 88% as the effective reinforcement ratio of single and hybrid bars increased, in comparison to steel-reinforced concrete beams cast using HPFRCC. Hybrid beams with an effective reinforcement ratio 1.35 times greater than the balancing ratio had a 23% improvement in displacement ductility and a 37.5% increase in ductility [78]. In contrast, the ductility index of fiber rebars that have been hardened with PET resin is about 33% lower than that of beam B0. This is likely because PET has a poor binding ability when combined with fiber ropes consisting of either glass or jute. Also, it is possible that the ductility index decreased due to the substitution of fiber rebars for steel bars in high-ratio construction. Concrete members that are reinforced with FRP bars usually have lower elastic modulus and linear-elastic behavior up to failure, hence the concrete members are less serviceable and have less ductility than regular reinforced-concrete (RC) members [79].

### 3.5 Failure modes

**Fig. 15** displays all possible failure mechanisms of the beams. After the tension reinforcing steel succumbed, the control specimens were crushed mid-span by compression concrete, which is the expected flexural failure mechanism. Several elements determine the manner of failure. These include the shear or flexural weakness of the section, the  $a/d$  ratio, the internal reinforcement, the cross-sectional area of the FRP, the FRP schemes and orientation, the anchoring system used, the quality of the strengthening material, and the integrity of the preparation [80, 81]. The failure in the EBR beams varied due to the different types of fiber sheets (GFT, JFT) and adhesive materials used (EP resins and GPP).

Beam failure as a result of bending is the most prevalent kind of failure. When the tensile strains are too great, the GFRP sheets will debond from the concrete, which is a common but undesirable outcome. Inadequate shear reinforcement or improper anchoring of the GFRP sheets might lead to shear failure [82]. No cracks were initially detected in the RC beams. The point load was the first point of failure for the beams, which occurred in the constant moment zone. Fractures continued to widen when the load was raised, and other fissures formed subsequent to the first crack. For beams B1 and B2 that strengthened externally with GFT layers, the failure mode was symmetrical regardless of the adhesive material. The cracks began at 8 kN then the cracks distributed at the flexural zone in the mid-span (one-third of span). The cracks were developed up to failure as tension failure at flexural zone. It can be seen that GFT sheets contribute to increasing the number of cracks which make beams a ductile behavior, that conforms with [83]. In the beam strengthened with JFT layers, the GPP exhibited more cracking compared to the installation using EP resin. The failure mode in the rebar beams was similar despite differences in the ultimate failure load. Overall, geopolymer paste showed better failure modes than epoxy resin due to its strong adhesion to the concrete surface and reduced shrinkage.

### 4 Conclusions

In this study, the feasibility of using geopolymer matrix as an environmentally friendly and cost-effective adhesive and reinforcing material alternative to epoxy materials was investigated. The practical results of the study yielded the following conclusions:

The environmental impact assessment of using GPP instead of EP resin represents a more environmentally friendly alternative with substantial benefits in terms of maintaining raw materials, reduced emissions, carbon footprint, waste utilization, and long-term sustainability.

The bonding material did not affect the ultimate load of the beams strengthened externally using GFT and JFT layers.

Utilizing jute textiles with epoxy gains the beam good beam behavior and prediction prior to failure due to the better bond efficiency between the jute textile and each EP and GPP.

The deformation beams include JFR were higher than those containing GFR due to the lower stiffness of JFR resulting from the strong bond between the GPP and the natural fiber surface.

The beams strengthened with fiber sheets (both GFT and JFT) using epoxy resin enhanced the toughness of RC beams. Based on these findings, epoxy seems to have superior flexural toughness compared to geopolymer.

Installing fiber laminates using GPP revealed good efficiency and higher toughness of RC beams by ratios of 58.9% and 49.2% than the control beam B0.

Beams strengthened with JFT exhibited higher ductility index compared to the control beam by 71.8% and 11.5% for adhesive EP and GPP, respectively. The GPP may need more treatment before loading test.

The GFT sheets contribute to increasing the number of cracks which make beams ductile behavior. On contrary the crack behavior of beams reinforced internally with 50% GFR or JFR.

### Acknowledgement

The writers gratefully acknowledge Ahmed Adel from Oretex for Chemicals and Glass Fiber Products and Mohamed Awad from Egypt Global Silicates company for their valuable assistance. Special thanks also go to Mostafa Saad, the laboratory supervisor of the Civil and Architectural Construction Department, Faculty of Technology and Education, Suez University.

### Funding Statement

The author(s) received no specific funding for this study.

### CRedit authorship contribution statement

**Marawan Ashraf Saad:** Conceptualization, Investigation, Formal analysis, Writing – original draft. **Bassam Abdelsalam Abdelsalam:** Conceptualization, Supervision, Investigation, Formal analysis, Writing – review & editing. **Omar Mohamed Omar Ibrahim:** Supervision, review & editing. **Hassan A. Mohamadien:** Supervision – review & editing.

### Conflicts of Interest

The authors declare that they have no conflicts of interest to report regarding the present study.

### Data Availability Statement

Some or all data, models, or codes that support the findings of this study are available from the corresponding author upon reasonable request.

### References

- [1] Zhang C, Li J, Yu M, Lu Y, Liu S. Mechanism and Performance Control Methods of Sulfate Attack on Concrete: A Review. *Materials* 2024; 17(19): 4836. <https://doi.org/10.3390/ma17194836>
- [2] Zhao Y, Xu X, Wang Y, Dong J. Characteristics of pitting corrosion in an existing reinforced concrete beam exposed to marine environment. *Construction and Building Materials* 2020; 234: 117392. <https://doi.org/10.1016/j.conbuildmat.2019.117392>
- [3] Fuhaid A F A, Niaz A. Carbonation and corrosion problems in reinforced concrete structures. *Buildings* 2022; 12(5): 586. <https://doi.org/10.3390/buildings12050586>
- [4] Xie M, Dangla P, Li K. Reactive transport modelling of concurrent chloride ingress and carbonation in concrete. *Materials and Structures* 2021; 54(5): 177. [https://doi.org/10.1617/s11527-021-01769-9\(0123456789\(\).,-volV\)](https://doi.org/10.1617/s11527-021-01769-9(0123456789().,-volV))
- [5] Diniță A, Ripeanu R G, Ilincă C N, Cursaru D, Matei D, Naim R I, Tănase M, Portoacă A I. Advancements in fiber-reinforced polymer composites: a comprehensive analysis. *Polymers* 2023; 16(1): 2. <https://doi.org/10.3390/polym16010002>
- [6] Yuan F, Xiong Y, Li P, Wu Y. Flexural behavior of seawater sea-sand coral aggregate concrete beams reinforced with FRP bars. *Journal of Composites for Construction* 2022; 26(6): 04022071. [https://doi.org/10.1061/\(ASCE\)CC.1943-5614.0001264](https://doi.org/10.1061/(ASCE)CC.1943-5614.0001264)
- [7] Serega S, Faustmann D H. Flexural strengthening of reinforced concrete beams using external tendons. *Engineering Structures* 2022; 252: 113277. <https://doi.org/10.1016/j.engstruct.2021.113277>
- [8] Mohammed A A, Manalo A C, Ferdous W, Zhuge Y, Vijay P, Pettigrew J. Experimental and numerical evaluations on the behaviour of structures repaired using prefabricated FRP composites jacket. *Engineering Structures* 2020; 210: 110358. <https://doi.org/10.1016/j.engstruct.2020.110358>

- [9] Wang Y, Zhong Y, Wan B, Zhang B, Wei Z, Bai Y. Axial compressive behavior and modeling of fiber-reinforced polymer-concrete-steel double-skin tubular stub columns with a rectangular outer tube and an elliptical inner tube. *Engineering Structures* 2022; 260: 114222. <https://doi.org/10.1016/j.engstruct.2022.114222>
- [10] Khatir A, Capozucca R, Khatir S, Magagnini E, Benaissa B, Cuong-Le T. An efficient improved Gradient Boosting for strain prediction in Near-Surface Mounted fiber-reinforced polymer strengthened reinforced concrete beam. *Frontiers of structural and civil engineering* 2024; 18(8): 1148-1168. <https://doi.org/10.1007/s11709-024-1079-x>
- [11] Nie X, Zhang S, Teng J. Strengths of RC beams with a fibre-reinforced polymer (FRP)-strengthened web opening. *Composite Structures* 2021; 258: 113380. <https://doi.org/10.1016/j.compstruct.2020.113380>
- [12] Reichenbach S, Preinstorfer P, Hammerl M, Kromoser B. A review on embedded fibre-reinforced polymer reinforcement in structural concrete in Europe. *Construction and Building Materials* 2021; 307: 124946. <https://doi.org/10.1016/j.conbuildmat.2021.124946>
- [13] Liu T, Tang J-T, Zhang S, Dong L, Hu L, Meng X, Zhao Y, Feng P. Carbon emissions of durable FRP composite structures in civil engineering. *Engineering Structures* 2024; 315: 118482. <https://doi.org/10.1016/j.engstruct.2024.118482>
- [14] Liang X, Wang W, Hu L, Feng P. Experimental and numerical study on high-temperature performance of prestressed CFRP-reinforced steel columns. *Engineering Structures* 2024; 301: 117347. <https://doi.org/10.1016/j.engstruct.2023.117347>
- [15] Nabil A, Afefy H M, Kassem N M. Ultimate capacity of reinforced concrete castellated beams subjected to external pre-stressing. *Engineering Structures* 2022; 250: 113471. <https://doi.org/10.1016/j.engstruct.2021.113471>
- [16] Tibhe S B, Rathi V R. Comparative experimental study on torsional behavior of RC beam using CFRP and GFRP fabric wrapping. *Procedia Technology* 2016; 24: 140-147. <https://doi.org/10.1016/j.protcy.2016.05.020>
- [17] Tworzewski P, Alexy J K, Barnes R W. Intermediate Crack Debonding of Externally Bonded FRP Reinforcement—Comparison of Methods. *Materials* 2022; 15(20): 7390. <https://doi.org/10.3390/ma15207390>
- [18] Sengun K, Arslan G. Parameters affecting the behaviour of RC beams strengthened in shear and flexure with various FRP systems: in *Structures Year; of Conference.*: Elsevier. <https://doi.org/10.1016/j.istruc.2022.04.024>
- [19] Salama A, Hawileh R, Abdalla J. Performance of externally strengthened RC beams with side-bonded CFRP sheets. *Composite Structures* 2019; 212: 281-290. <https://doi.org/10.1016/j.compstruct.2019.01.045>
- [20] Hawileh R, Nawaz W, Abdalla J. Flexural behavior of reinforced concrete beams externally strengthened with Hardwire Steel-Fiber sheets. *Construction and Building Materials* 2018; 172: 562-573. <https://doi.org/10.1016/j.conbuildmat.2018.03.225>
- [21] Ivanova I, Assih J, Dontchev D. Application of natural fiber composite materials in the strengthening of reinforced concrete structures: in *IOP Conference Series: Materials Science and Engineering Year; of Conference.*: IOP Publishing. 10.1088/1757-899X/951/1/012012
- [22] Alam M A, Onik S A, Mustapha K N B. Crack based bond strength model of externally bonded steel plate and CFRP laminate to predict debonding failure of shear strengthened RC beams. *Journal of Building Engineering* 2020; 27: 100943. <https://doi.org/10.1016/j.jobbe.2019.100943>
- [23] Nayak A, Kumari A, Swain R. Strengthening of RC beams using externally bonded fibre reinforced polymer composites: in *Structures Year; of Conference.*: Elsevier. <https://doi.org/10.1016/j.istruc.2018.03.004>
- [24] Zhang F, Dai J-G, Wang Z, Wang M, Leng Y, Xu Q. Bond durability of epoxy and cement-bonded CFRP reinforcement to concrete interfaces subject to water immersion. *Materials and Structures* 2021; 54: 1-12. [https://doi.org/10.1617/s11527-021-01769-9\(0123456789\),-volV](https://doi.org/10.1617/s11527-021-01769-9(0123456789),-volV)
- [25] Wang Z, Dai J-G, Wang M, Chen L, Zhang F, Xu Q. Residual bond strengths of epoxy and cement-bonded CFRP reinforcements to concrete interfaces after elevated temperature exposure. *Fire Safety Journal* 2021; 124: 103393. <https://doi.org/10.1016/j.firesaf.2021.103393>
- [26] Tetta Z C, Koutas L N, Bournas D A. Textile-reinforced mortar (TRM) versus fiber-reinforced polymers (FRP) in shear strengthening of concrete beams. *Composites Part B: Engineering* 2015; 77: 338-348. <https://doi.org/10.1016/j.compositesb.2015.03.055>
- [27] Almutairi A L, Tayeh B A, Adesina A, Isleem H F, Zeyad A M. Potential applications of geopolymers in construction: A review. *Case Studies in Construction Materials* 2021; 15: e00733. <https://doi.org/10.1160/j.cscm.2021.e00733>
- [28] Zhang Y, Li X, Zhu Y, Shao X. Experimental study on flexural behavior of damaged reinforced concrete (RC) beam strengthened by toughness-improved ultra-high performance concrete (UHPC) layer. *Composites Part B: Engineering* 2020; 186: 107834. <https://doi.org/10.1016/j.compositesb.2020.107834>
- [29] Koutas L N, Papakonstantinou C G. Flexural strengthening of RC beams with textile-reinforced mortar

- composites focusing on the influence of the mortar type. *Engineering Structures* 2021; 246: 113060. <https://doi.org/10.1016/j.engstruct.2021.113060>
- [30] Zhang H Y, Liu H Y, Kodur V, Li M Y, Zhou Y. Flexural behavior of concrete slabs strengthened with textile reinforced geopolymer mortar. *Composite Structures* 2022; 284: 115220. <https://doi.org/10.1016/j.compstruct.2022.115220>
- [31] Azam R, Soudki K, West J S, Noël M. Strengthening of shear-critical RC beams: Alternatives to externally bonded CFRP sheets. *Construction and Building Materials* 2017; 151: 494-503. <https://doi.org/10.1016/j.conbuildmat.2017.06.106>
- [32] Attia M M, Abdelsalam B A, Tobbala D E, Rageh B O. Flexural behavior of strengthened concrete beams with multiple retrofitting systems. *Case Studies in Construction Materials* 2023; 18: e01862. <https://doi.org/10.1016/j.cscm.2023.e01862>
- [33] Attia M M, Abdelsalam B A, Eita M, Ahmed M, Liang Q Q, Rageh B O. Tests and finite element modeling of concrete beams reinforced with reused steel bars. *Structural Concrete* 2024; 25(1): 137-153. <https://doi.org/10.1002/suco.202300316>
- [34] Junaid M T, Elbana A, Altoubat S. Flexural response of geopolymer and fiber reinforced geopolymer concrete beams reinforced with GFRP bars and strengthened using CFRP sheets: in *Structures Year; of Conference.*: Elsevier. <https://doi.org/10.1016/j.istruc.2020.02.003>
- [35] Saad M, Agwa I S, Abdelsalam Abdelsalam B, Amin M. Improving the brittle behavior of high strength concrete using banana and palm leaf sheath fibers. *Mechanics of advanced materials and structures* 2022; 29(4): 564-573. <https://doi.org/10.1080/15376494.2020.1780352>
- [36] Zheng A, Liu Z, Li F, Li S. Experimental investigation of corrosion-damaged RC beams strengthened in flexure with FRP grid-reinforced ECC matrix composites. *Engineering Structures* 2021; 244: 112779. <https://doi.org/10.1016/j.engstruct.2021.112779>
- [37] Sneed L, D'Antino T, Carloni C, Pellegrino C. A comparison of the bond behavior of PBO-FRCM composites determined by double-lap and single-lap shear tests. *Cement and Concrete Composites* 2015; 64: 37-48. <https://doi.org/10.1016/j.cemconcomp.2015.07.007>
- [38] Raoof S M, Bournas D A. TRM versus FRP in flexural strengthening of RC beams: Behaviour at high temperatures. *Construction and building materials* 2017; 154: 424-437. <https://doi.org/10.1016/j.conbuildmat.2017.07.195>
- [39] Dong K, Sui Z-a, Kexu H, Jiang J, Derun D. Experiment Study on Flexural Behavior of Fire Damaged Prefabricated Hollow Slab Strengthened by CFRP and TRM: in *IOP Conference Series: Earth and Environmental Science Year; of Conference.*: IOP Publishing. DOI10.1088/1755-1315/267/3/032064
- [40] Xu J, Tan C, Aboutaha R. Experimental investigation of high strength reinforced concrete columns damaged by fire and retrofitted with CFRP jackets: in *IOP Conference Series: Earth and Environmental Science Year; of Conference.*: IOP Publishing. DOI10.1088/1755-1315/358/4/042009
- [41] Farhan N A, Sheikh M N, Hadi M N. Investigation of engineering properties of normal and high strength fly ash based geopolymer and alkali-activated slag concrete compared to ordinary Portland cement concrete. *Construction and Building Materials* 2019; 196: 26-42. <https://doi.org/10.1016/j.conbuildmat.2018.11.083>
- [42] Amran M, Debbarma S, Ozbakkaloglu T. Fly ash-based eco-friendly geopolymer concrete: A critical review of the long-term durability properties. *Construction and Building Materials* 2021; 270: 121857. <https://doi.org/10.1016/j.conbuildmat.2020.121857>
- [43] Hassan A, Arif M, Shariq M. Use of geopolymer concrete for a cleaner and sustainable environment—A review of mechanical properties and microstructure. *Journal of cleaner production* 2019; 223: 704-728. <https://doi.org/10.1016/j.jclepro.2019.03.051>
- [44] Kumar M L, Revathi V. Microstructural properties of alkali-activated metakaolin and bottom ash geopolymer. *Arabian Journal for Science and Engineering* 2020; 45(5): 4235-4246. <https://doi.org/10.1007/s13369-020-04417-6>
- [45] Li J, Zha W, Lv W, Xu T, Wang B, Wang B. Mechanical properties and sulfate resistance of basalt fiber-reinforced alkali-activated fly ash-slag-based coal gangue pervious concrete. *Case Studies in Construction Materials* 2024; 21: e03961. <https://doi.org/10.1016/j.cscm.2024.e03961>
- [46] Sasui S, Kim G, Nam J, Koyama T, Chansomsak S. Strength and microstructure of class-C fly ash and GGBS blend geopolymer activated in NaOH & NaOH+ Na<sub>2</sub>SiO<sub>3</sub>. *Materials* 2019; 13(1): 59.
- [47] De Azevedo A R, Teixeira Marvila M, Barbosa de Oliveira L, Macario Ferreira W, Colorado H, Rainho Teixeira S, Mauricio Fontes Vieira C. Circular economy and durability in geopolymers ceramics pieces obtained from glass polishing waste. *International Journal of Applied Ceramic Technology* 2021; 18(6): 1891-1900. <https://doi.org/10.1111/ijac.13780>
- [48] de Azevedo A R, Marvila M T, Ali M, Khan M I, Masood F, Vieira C M F. Effect of the addition and processing of glass polishing waste on the durability of geopolymeric mortars. *Case Studies in Construction Materials* 2021; 15: e00662. <https://doi.org/10.1016/j.cscm.2021.e00662>
- [49] Marvila M T, Azevedo A R, Delaqua G C, Mendes B C, Pedroti L G, Vieira C M. Performance of geopolymer

- tiles in high temperature and saturation conditions. *Construction and Building Materials* 2021; 286: 122994. <https://doi.org/10.1016/j.conbuildmat.2021.122994>
- [50] Amin M, Abdelsalam B A. Efficiency of rice husk ash and fly ash as reactivity materials in sustainable concrete. *Sustainable Environment Research* 2019; 29(1): 1-10. <https://doi.org/10.1186/s42834-019-0035-2>
- [51] Singh N B, Middendorf B. Geopolymers as an alternative to Portland cement: An overview. *Construction and Building Materials* 2020; 237: 117455. <https://doi.org/10.1016/j.conbuildmat.2019.117455>
- [52] Albidah A, Abadel A, Alrshoudi F, Altheeb A, Abbas H, Al-Salloum Y. Bond strength between concrete substrate and metakaolin geopolymer repair mortars at ambient and elevated temperatures. *Journal of Materials Research and Technology* 2020; 9(5): 10732-10745. <https://doi.org/10.1016/j.jmrt.2020.07.092>
- [53] Aiken T A, Kwasny J, Sha W, Tong K T. Mechanical and durability properties of alkali-activated fly ash concrete with increasing slag content. *Construction and Building Materials* 2021; 301: 124330. <https://doi.org/10.1016/j.conbuildmat.2021.124330>
- [54] Amin M, Zeyad A M, Tayeh B A, Agwa I S. Effect of high temperatures on mechanical, radiation attenuation and microstructure properties of heavyweight geopolymer concrete. *Structural Engineering and Mechanics, An Int'l Journal* 2021; 80(2): 181-199. <https://doi.org/10.12989/sem.2021.80.2.181>
- [55] Tayeh B A, Zeyad A M, Agwa I S, Amin M. Effect of elevated temperatures on mechanical properties of lightweight geopolymer concrete. *Case Studies in Construction Materials* 2021; 15: e00673. <https://doi.org/10.1016/j.cscm.2021.e00673>
- [56] Amin M, Elsakhawy Y, Abu el-hassan K, Abdelsalam B A. Behavior evaluation of sustainable high strength geopolymer concrete based on fly ash, metakaolin, and slag. *Case Studies in Construction Materials* 2022; 16: e00976. <https://doi.org/10.1016/j.cscm.2022.e00976>
- [57] ASTM A S. Standard Specification for Portland Cement. ASTM C150/C150M-19a. 2019.
- [58] Subcommittee A. C09. 20: "Standard Specification for Concrete Aggregates (ASTM C33/C33M-18)". ASTM International, West Conshohocken, PA, USA 2018.
- [59] Standard A. C494/C494M-17; Standard Specification for Chemical Admixtures for Concrete. ASTM: West Conshohocken, PA, USA 2020.
- [60] Committee A. Guide for selecting proportions for high-strength concrete using portland cement and other cementitious materials: in Year; of Conference.: American Concrete Institute.
- [61] ASTM A. C881 Standard Specification for Epoxy-Resin-Base Bonding Systems for Concrete. American Society for Testing and Materials: West Conshohocken, PA, USA 2015.
- [62] Subcommittee A. ASTM C618-19, "Standard Specification for Coal Fly Ash and Raw or Calcined Natural Pozzolan for Use in Concrete. 2019.
- [63] Standard A. D7205/D7205M-06. Standard Test Method for Tensile Properties of Fiber Reinforced Polymer Matrix Composite Bars", ASTM International, West Conshohocken, PA 2016.
- [64] EN B. 1542—Products and Systems for the Protection and Repair of Concrete Structures-Test Methods-Measurement of Bond Strength by Pull-Off. British Standard Institution, London 1999.
- [65] Committee E-P. ECP-203: 2007-Egyptian Code for design and construction of concrete structures. HBRC, Giza 2007.
- [66] International A. ASTM D7205/D7205M-06: Standard Test Method for Tensile Properties of Fiber Reinforced Polymer Matrix Composite Bars: in Year; of Conference.: American Society for Testing and Materials West Conshohocken, PA, USA.
- [67] EN B. 15422: 2008 Precast concrete products. Specification of glass fibres for reinforcement of mortars and concretes.
- [68] ACI Committee. Building code requirements for structural concrete (ACI 318-08) and commentary: in Year; of Conference.: American Concrete Institute.
- [69] Alkhrdaji T, Fyfe E R, Korff J, Schupack M, Bakis C E, Gentry T R, Lee M W, Scott D W, Balaguru P, Gergely J. Guide for the design and construction of structural concrete reinforced with FRP bars. *Proceedings of the American Concrete Institute (ACI) committee* 2006; 440.
- [70] ASTM, ASTM C78-02 Standard Test Method for Flexural Strength of Concrete (Using Simple Beam with Third-Point Loading). 2002.
- [71] Deng J, Zhong M, Zhang Z, Zhu M. Ultimate and Deflection Performance of Concrete Beams Strengthened in Flexure with Basalt-Textile-Reinforced Polymer Mortar. *Polymers* 2023; 15(2): 445. <https://doi.org/10.3390/polym15020445>
- [72] Nawaz W, Elchalakani M, Karrech A, Yehia S, Yang B, Youssf O. Flexural behavior of all lightweight reinforced concrete beams externally strengthened with CFRP sheets. *Construction and Building Materials* 2022; 327: 126966. <https://doi.org/10.1016/j.conbuildmat.2022.126966>
- [73] Xu F, Chen Y, Zheng X, Ma R, Tian H. Experimental study on corrosion and mechanical behavior of main cable wires considering the effect of strain. *Materials* 2019; 12(5): 753. <https://doi.org/10.3390/ma12050753>
- [74] C A, Standard test method for flexural toughness and first-crack strength of fiber-reinforced concrete (using beam with third-point loading), ASTM International West Conshohocken, PA. 1997. 1-8.

- [75] Ibrahim A A, Rasheed M M. The effect of compression reinforcement on the shear behavior of concrete beams with hybrid reinforcement. *Journal of Building Pathology and Rehabilitation* 2025; 10(1): 8. <https://doi.org/10.1007/s41024-024-00502-7>
- [76] Meng D, Lee C K, Zhang Y, Structural behavior of reinforced polyvinyl alcohol engineered cementitious composite (PVA-ECC) beams under static and fatigue loadings, in *Advances in engineered cementitious composites*, Elsevier. 2022. 161-208. <https://doi.org/10.1016/B978-0-323-85149-7.00012-4>
- [77] Mahalingam M, Rao R P N, Kannan S. Ductility behavior fiber reinforced concrete beams strengthened with externally bonded glass fiber reinforced polymer laminates. *American Journal of Applied Sciences* 2013; 10 (1): 107. <https://doi.org/10.3844/ajassp.2013.107.111>
- [78] Sijavandi K, Sharbatdar M K, Kheyroddin A. Experimental evaluation of flexural behavior of high-performance fiber reinforced concrete beams using GFRP and high strength steel bars: in *Structures Year; of Conference.*: Elsevier. <https://doi.org/10.1016/j.istruc.2021.07.020>
- [79] Maranan G, Manalo A, Benmokrane B, Karunasena W, Mendis P, Nguyen T. Flexural behavior of geopolymer-concrete beams longitudinally reinforced with GFRP and steel hybrid reinforcements. *Engineering Structures* 2019; 182: 141-152. <https://doi.org/10.1016/j.engstruct.2018.12.073>
- [80] Saribiyik A, Abodan B, Balci M T. Experimental study on shear strengthening of RC beams with basalt FRP strips using different wrapping methods. *Engineering Science and Technology, an International Journal* 2021; 24(1): 192-204. <https://doi.org/10.1016/j.jestch.2020.06.003>
- [81] Askar M K, Hassan A F, Al-Kamaki Y S. Flexural and shear strengthening of reinforced concrete beams using FRP composites: A state of the art. *Case Studies in Construction Materials* 2022; 17: e01189. <https://doi.org/10.1016/j.cscm.2022.e01189>
- [82] Sallal A K, Rajan A. Flexural behavior of reinforced concrete beams strengthening with glass fiber reinforced polymer (GFRP) at different sides. *International Journal of Science and Research (IJSR)* 2016; 5(5): 1837-1843.
- [83] Yu T, Li C, Lei J, Zhang H. Fatigue of concrete beams strengthened with glass-fiber composite under flexure. *Journal of Composites for Construction* 2011; 15(4): 557-564. [https://doi.org/10.1061/\(ASCE\)CC.1943-5614.0000189](https://doi.org/10.1061/(ASCE)CC.1943-5614.0000189)